Engineering Failure Analysis 34 (2013) 24–34

Contents lists available at ScienceDirect

Engineering Failure Analysis

journal homepage: www.elsevier.com/locate/engfailanal

Using FEM to determine the thermo-mechanical stress in tube to tube–sheet joint for the SCC failure analysis

Shugen Xu [a,b,*], Yanling Zhao [a]

[a] College of Chemical Engineering, China University of Petroleum (Huadong), Qingdao 266580, China
[b] State Key Laboratory of Heavy Oil Processing, China University of Petroleum (Huadong), Qingdao 266580, China

ARTICLE INFO

Article history:
Received 1 April 2013
Received in revised form 16 July 2013
Accepted 16 July 2013
Available online 25 July 2013

Keywords:
Finite element analysis
Thermo-mechanical stresses
SCC
Tube to tube–sheet joint

ABSTRACT

The stress corrosion cracking in a weld of the tube to tube–sheet region of heat exchangers is a common problem. Thermo-mechanical stress in tube to tube–sheet joints including welding effect should be determined in this situation for failure analysis. In this paper, the Finite Element Method (FEM) is used to predict the thermo-mechanical stresses including welding residual stress in a tube to tube–sheet weld. Both the thermo-mechanical stress distribution with and without the welding residual stress have also been investigated by numerical simulation. The welding, operating temperature, and operating pressure have effect on total stresses. Especially, the welding residual stresses play an important role in total stress state in tube to tube–sheet joints. Geometric discontinuities of the vicinity of gap cause the welding joint to experience a local stress concentration. A high tensile stress in the tube to tube–sheet region has been demonstrated by FEM, which is the stress aspect for the SCC phenomenon of austenitic stainless steel in chloride environment.

1. Introduction

The shell–tube heat exchanger is widely used in process industries. The tube to tube–sheet joint is a critical element of shell–tube heat exchangers. The joint is made by either expansion, welding or a combination of them [1]. Sometimes, the tube is made of austenitic stainless steel for anti-corrosion. The tube–sheet with surface welding consisting of a thin layer of austenitic stainless steel onto a lower cost, thicker base metal, has been widely used in construction of corrosion resistant equipment. It not only has good resistance to corrosion but also can meet the strength requirement [2].

The interfaces between tube and tube–sheet are particularly difficult to test, because of high temperature and large temperature gradients, as well as the complicate geometry [3]. The crack development in welds of the tube to tube–sheet region of the heat exchanger is a common problem. Such crack is propagated by stress corrosion cracking or thermal fatigue, or localized corrosion [4]. The local stress levels, arising from a combination of the applied loading, as well as thermal and residual stresses, contribute to the failure scenario. The SCC of austenitic stainless steels may occur when an alloy is simultaneously subject to the tensile stress and a specific corrosive medium. The residual stresses associated with welding of tube to tube–sheet can play a major role in this situation [5]. Thus, in addition to paying more attention to material and environment, a good prediction of thermo-mechanical stress under operating temperature and pressure including the welding residual stress is necessary [6].

* Corresponding author at: College of Chemical Engineering, China University of Petroleum (Huadong), Qingdao 266580, China. Tel.: +86 532 8698 3482; fax: +86 532 8698 3480.
E-mail address: xsg123@163.com (S. Xu).

1350-6307/$ - see front matter © 2013 Elsevier Ltd. All rights reserved.
http://dx.doi.org/10.1016/j.engfailanal.2013.07.011

The stress, including thermal stress, mechanical stress, and welding residual stress of tube to tube–sheet has received a lot of attention in recent years. Tait and press [7] studied an experimental method to obtain the residual stresses in tube to tube–sheet welds of industrial boilers. Meraha et al. [8]investigated the effect of initial radial clearance and material strain hardening on the strength of the expanded tube to tube–sheet joint by using the FEM. With the development of computer technology, FEM has been confirmed to be a useful and powerful numerical analysis tool to predict the welding residual stress [9–11]. The author has predicted the residual stresses in a tube to tube sheet weld. The effect of heat input, preheating temperature, and gap between tube and tube hole on residual stresses was also investigated by numerical simulation [12].

In this paper, a failure case of a tube–sheet has been reviewed. The crack appearance indicated that the failure occurred by SCC. However, the stress distribution in the crack initiation zone was not clear. It is also not clear how the welding residual stress affected the total stress quantitatively during the operation. This will be discussed in this paper, aiming to provide a reference for analyzing the SCC failure of the tube to tube–sheet joint.

2. The SCC in tube–sheet

A tube-shell heat exchanger is used in an ammonia plant. The operating pressure and temperature of the shell side are 2.8 MPa and 340 °C, respectively. The operating medium is steam. The operating pressure and temperature of the tube side are 31.4 MPa and 380 °C, respectively. The operating medium is mixed including H_2, N_2, CH_4, Ar, and NH_3. The tube size is $\varnothing 35 \times 6.5$ mm. The base of tube–sheet is manufactured from a type of low alloy steel, Q345R, which is a Chinese steel grade. The tube and surface welding layer is manufactured from type 1Cr18Ni9 austenitic stainless steel, a Chinese steel grade, which is equivalent to type 304, and used for the requirements of corrosion resistance. The tube to tube–sheet joint consisted of an internal groove weld and an external fillet weld. The welding joint is not only for the strength connection, but also for the sealing. The gap between tube and tube–sheet hole is inevitable due to the short of tube expansion during fabrication [2]. A diagram of the tube–sheet section is shown in Fig. 1.

Cracking was apparent on the tube to tube–sheet joint, adjacent to the tube end. Some reddish points are present on the surface during die penetrant examination, but no gross mechanical damage, yielding, or weld defects are evident.

In order to find out the crack initiation location, the crack appearance in different sections in different depths was checked. The crack in the tube to tube–sheet surface appeared to be two pinholes, as shown in Fig. 2(a). As the region was ground, the length of crack increased, as shown in Fig. 2(b). After the third attempt at grinding, the crack became significantly longer. The main cracks and branching of cracks can be observed clearly, as shown in Fig. 2(c). After the final attempt at grinding the crack out, the branches disappeared, and the main crack become longer, as shown in Fig. 2(d). The diagram of the tube to tube–sheet region that leaked during service is shown in Fig. 3. It can be seen that the cracks originated from the vicinity of gap between tube and tube–sheet hole at the root of the weld.

The chemical composition of the tube and surface welding layer were consistent with a type 1Cr18Ni9 austenitic stainless steel. No compositional anomalies were detected. Energy-spectrum scanning analysis of the corrosion product on the crack surfaces revealed chlorine, sulfide, and oxygen in addition to the base metal elements.

A metallographic cross section through the most severe cracking is shown in Fig. 4. Branching, transgranular cracking is evident, emanating primarily from the interface between base metal and surface welding layer.

The analytical investigation concluded that the tube to tube–sheet failed as a result of stress-corrosion cracking (SCC) that initiated at the shell side. Steam containing chlorine, may have leaked from the boiler water, and combined with the inherent susceptibility of the material and tensile stress. These factors combined synergistically to result in cracking. Aqueous chlorides, especially within an acidic environment, have been shown to cause SCC in austenitic stainless steels under tensile stress [13]. The use of a type of 18-8 austenite stainless steel, 1Cr18Ni9 to prevent internal corrosion damage did not

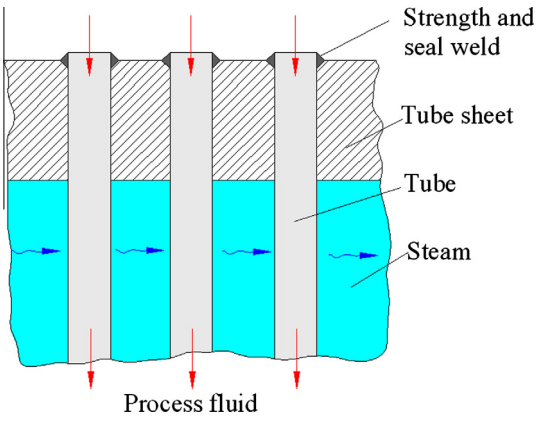

Fig. 1. Diagram of the tube to tube–sheet joint zone.

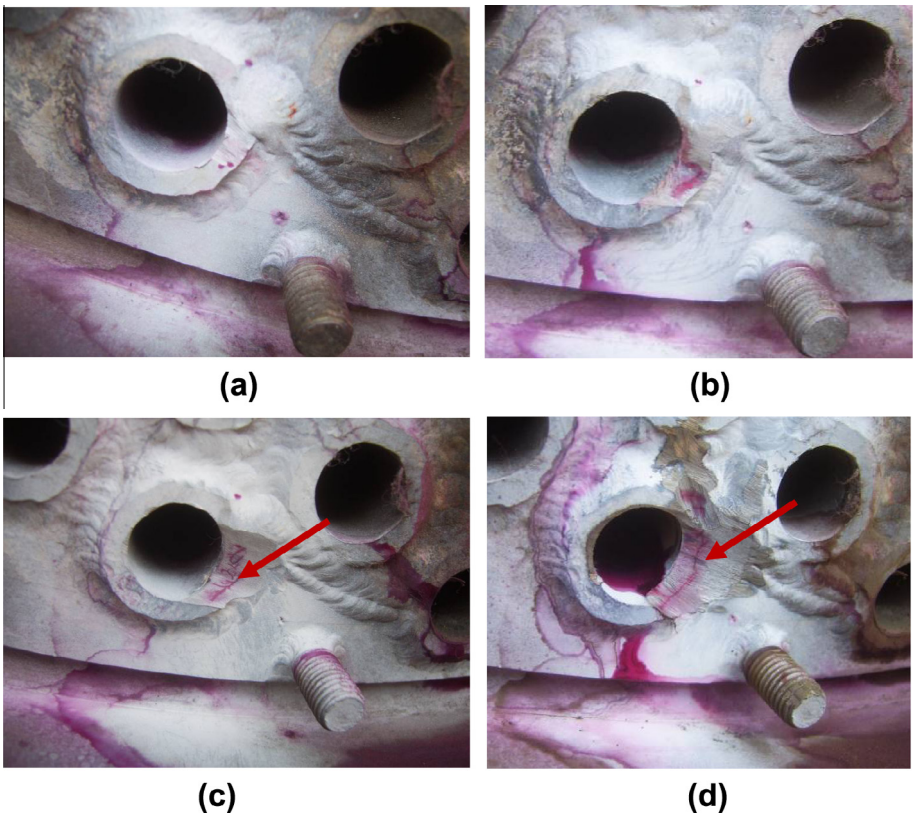

Fig. 2. Crack appearance in tube to tube–sheet region. (a) 1st grinded, the crack looks like two pinholes, (b) 2nd grinded, the crack is clear, (c) 3rd grinded, Main cracks and branching of cracks and (d) 4th grinded, the crack is longest of all.

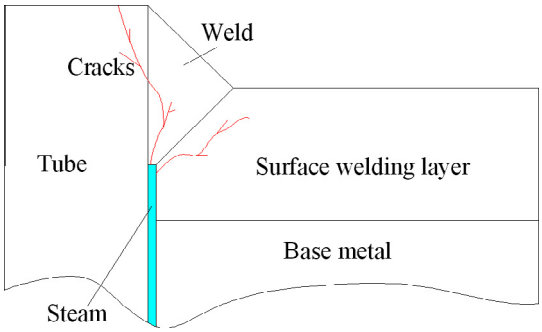

Fig. 3. Diagram of the tube to tube–sheet region that leaked during service.

adequately foresee the potential for corrosion damage from external contamination. This conclusion should be supported by the tensile stress. The operating stresses including residual stresses from fabrication and welding is complicated. Therefore, the Finite Element Method (FEM) is employed to predict the stress in the following sections.

3. FE analysis of the stress in tube to tube–sheet joint

3.1. Geometrical model and meshing

The geometrical model of the tube to tube–sheet joint is shown in Fig. 5. The thickness of base metal and surface welding layer metal are 230 mm and 6 mm, respectively. The weld geometry is shown in Fig. 5, and the gap between the tube and tube hole is 0.2 mm. For the ease of calculation, a part of the tube–sheet is selected for the FE analysis. Although the real structural stress analysis is a 3-D procedure, it is often considered sufficient to represent a circumferential weld with an

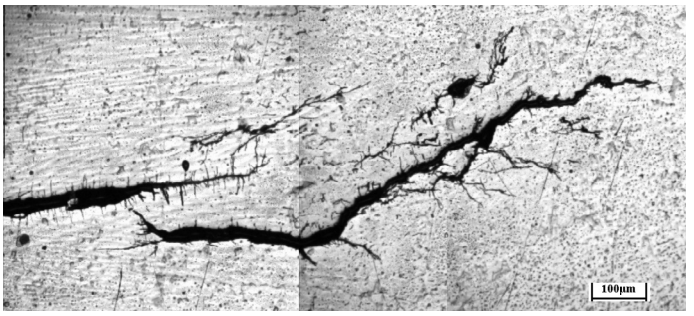

Fig. 4. Metallographic cross section through the cracked region of the tube to tube–sheet joint, showing branching cracks.

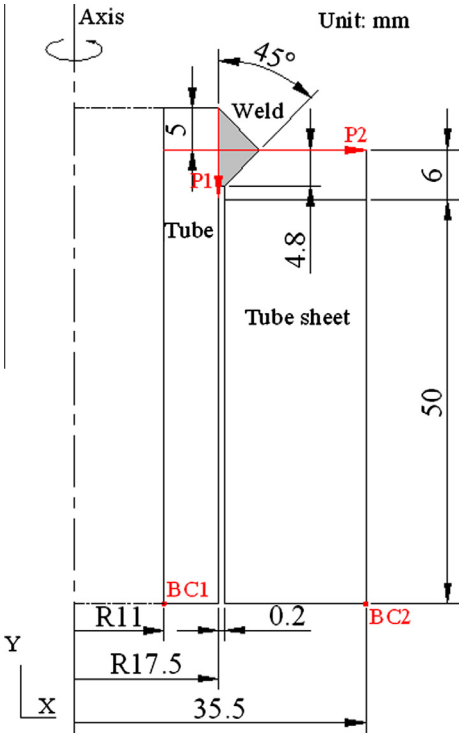

Fig. 5. The geometrical model of tube to tube–sheet weld.

axi-symmetric FE model. Therefore, the methodology described here is based on an axi-symmetric model. A 2-D axi-symmetric model is established and the FE meshing is shown in Fig. 6. In total, 4024 nodes and 3800 elements are meshed. In order to analyze the results, two reference paths named P1 and P2 are defined as shown in Fig. 5. P1 is along the interface between the tube surface and the weld, P2 is crossing through the whole thickness of the tube, and along the tube–sheet surface.

3.2. Material properties

The chemical compositions of 1Cr18Ni9 and Q345R steel are listed in Ref. [2,14]. For thermal and mechanical analysis, temperature-dependent thermo-physical and mechanical properties of the materials are incorporated, as listed in Ref. [15].

3.3. Stress analysis

3.3.1. Welding residual stress analysis

A sequential coupling thermal–structural analysis program is developed to calculate the welding temperature and residual stress by FE software ABAQUS. The thermal analysis is carried out to obtain the welding temperature history firstly, and

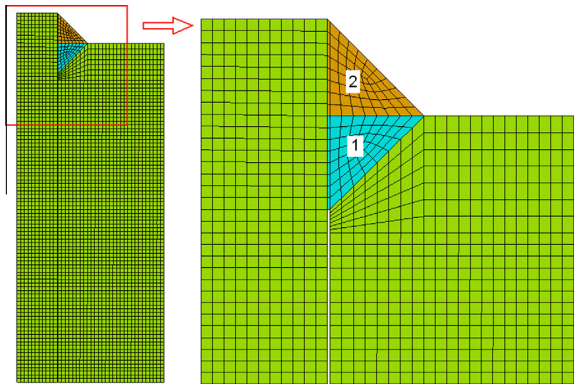

Fig. 6. FE mesh of the model.

then the temperature results are applied incrementally to the structural model to calculate the residual stress. The detailed calculation methods and results are available in Ref. [12].

3.3.2. Thermo-mechanical stress under operating temperature and pressure

3.3.2.1. Formulation of thermo-mechanical stress. In the stress analysis, displacements are stored by the finite element software at the nodal positions as a solution variable, and loads are defined as prescribed displacements and forces. Employing the interpolation functions, it is possible to calculate the strain and the stress increments at any point within the element using the compatibility and constitutive equations. The software transforms the mechanical equilibrium equations into a set of simultaneous equations, so that the nodal displacements and forces are related to each other through the elemental stiffness matrix [16,17].

The resulting total strain vector, $\{\Delta\varepsilon\}$, may be expressed as follows:

$$\{\Delta\varepsilon\} = \{\Delta\varepsilon^{el}\} + \{\Delta\varepsilon^{th}\} + \{\Delta\varepsilon^{pl}\} \tag{1}$$

where $\{\Delta\varepsilon^{el}\}$ is the elastic strain increment vector, $\{\Delta\varepsilon^{th}\}$ is the thermal strain increment vector, and $\{\Delta\varepsilon^{pl}\}$ is the plastic strain increment vector. Depending on the mathematical construct used to describe the constitutive behavior of the material, one or more of the elastic, plastic components would appear in the thermal–mechanical stress analysis.

The incremental strains within an element can be expressed in terms of the incremental element nodal displacements as

$$\{\Delta\varepsilon\} = [B]\{\delta\}^{e} \tag{2}$$

where $[B]$ is the strain–displacement interpolation matrix and $\{\delta\}^{e}$ is displacement vector for element (e).

The elastic strain increment vector $\{\Delta\varepsilon^{el}\}$ is related to the stress increment vector $\{\Delta\sigma^{el}\}$ by Hooke's law:

$$\{\Delta\sigma^{el}\} = [D]\{\Delta\varepsilon^{el}\} \tag{3}$$

where $[D]$ is contains the elastic constants related to temperature-dependent elastic modulus E and Poisson's ratio μ.

The incremental thermal strain vector $\{\Delta\varepsilon^{th}\}$ arises from the volume changes that accompany the temperature increment ΔT, which is calculated by the thermal analysis. It is normally formulated by a temperature-dependent differential thermal expansion coefficient, α ($^{\circ}C^{-1}$):

$$\{\Delta\varepsilon^{th}\} = [\alpha]\Delta T \tag{4}$$

However, ABAQUS uses a temperature-dependent total thermal strain coefficient, α^0 ($^{\circ}C^{-1}$). The differential and total thermal expansion coefficients are related to each other through:

$$\alpha^0(T) = \frac{1}{T - T^0}\int_{T^0}^{T} \alpha(T)\mathrm{d}T \tag{5}$$

where T^0 is a reference temperature designating the point at which the material exhibits no dilatational strain. A description of the variation in α^0 with temperature used in the analysis and the rationalization for the approach adopted is given in the section below on thermo-mechanical properties.

3.3.2.2. Loading and boundary conditions. The operating temperature of shell side and tube side are 340 °C and 380 °C, respectively. The initial temperature is 20 °C. The temperature field is calculated firstly, and then the temperature results are applied to the structural model to calculate the thermal stress. The thermal stress is calculated using temperature-dependent coefficient of thermal expansion. Hence, the final stresses are only generated due to the heating of the whole model from the reference temperature to the operating temperature.

The operating pressure of shell side and tube side are 2.8 MPa and 31.4 MPa, respectively. Therefore, the mechanical stresses will be generated during service. The mechanical stresses were analyzed numerically ignoring the influence of welding and operating temperature. The pressure of tube side, $p_{shell} = 2.8$ MPa was applied on the inner surface of tube, tube end section, outer surface of weld, and the outer surface of tube–sheet. The pressure of shell side, $p_{tube} = 31.4$ MPa was applied on the gap between the tube and tube–sheet hole, which adjacent to the shell during operating time, as shown in Fig. 7. The boundary conditions for the FE model are illustrated in Fig. 10. The node BC1 and BC2 is constrained in both x-direction and y-direction, that is $u_x = u_y = 0$.

3.3.3. Thermo-mechanical stress taking residual stress into consideration

The welding residual stress and thermo-mechanical stress under operating temperature and pressure are analyzed above. In fact, the real stress state in tube to tube–sheet region is the thermo-mechanical stress combined with welding residual stress. Two analysis steps are established in ABAQUS software. The first step is established for the analysis of welding residual stress, and second step is established for the analysis of thermo-mechanical stress with the influence of residual stress that developed in the first step.

4. Calculation results

4.1. Thermo-mechanical stress distribution without welding effect

The thermo-mechanical stress contours of radial stress, axial stress and hoop stress is shown in Fig. 8. The peak stresses of radial stress, axial stress and hoop stress are 34.6 MPa, −8.12 MPa, and 62.1 MPa. The stress in the zone that around the end of gap is compressive. Compared to the welding residual stress, the thermo-mechanical stress under operating temperature and pressure is low. It also can be seen that the stresses in surface welding layer and base metal are not continuous. The mismatching of yield strength between base metal and surface welding layer caused an unbalanced distribution of residual stresses.

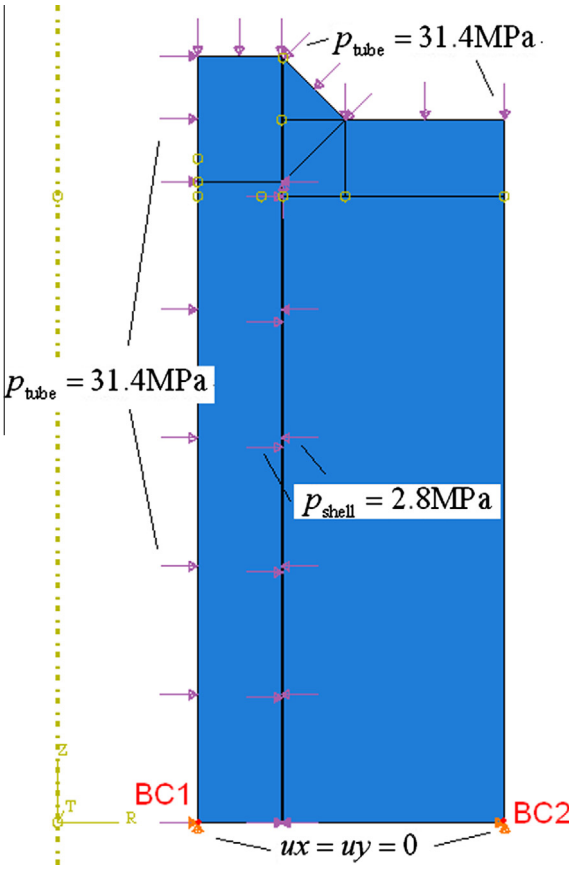

Fig. 7. Mechanical load and boundary conditions for the stress analysis.

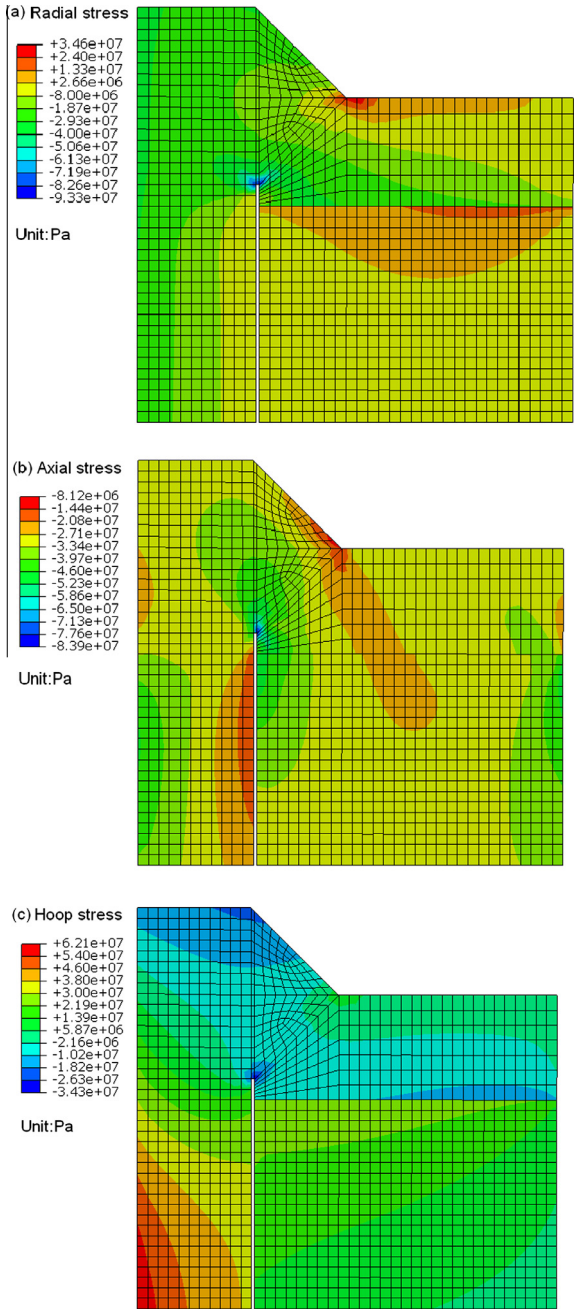

Fig. 8. The contours of thermo-mechanical stress without welding effect: radial stress (a), axial stress (b), hoop stress (c).

Fig. 9 shows the stress distribution along P1 and P2. All the stress components have the similar trend along P1, as shown in Fig. 10(a). Along the weld edge, all the stresses increase firstly, and then decrease to the lowest level. Along the HAZ, the radial stress is 0 MPa approximately. The axial stress is compressive and keeps constant along the HAZ. The hoop stress is tensile, and increases to 35.0 MPa at 18.2 mm from the initial point.

Along P2, The radial stress is increased gradually from the inner surface of the tube and reaches the peak (182 MPa) at weld root, and then it is decreased away from the weld root. The axial and hoop stresses are decreased from inner surface of the tube and reach the minimum value at the outer surface of tube, then the stress are increased and reach the peak value at the weld root, and then they are decreased away from the weld root.

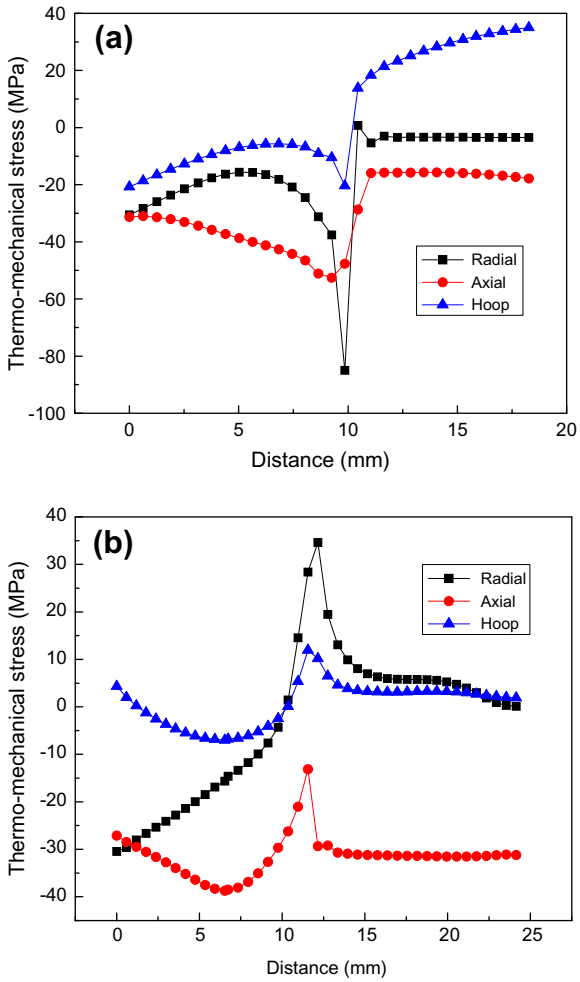

Fig. 9. The distributions of thermo-mechanical stresses without welding effect along P1 (a) and P2 (b).

4.2. Thermo-mechanical stress distribution including welding effect

Fig. 10 shows the stress contours of radial stress, axial stress and hoop stress under the operating temperature and pressure including the welding effect. It is shown that large tensile residual stresses are generated on the weld metal and HAZ. As is shown, the peak stresses of radial stress, axial stress and hoop stress are 340, 171 and 377 MPa. The peak stress of radial stress is located on the weld root, while axial stress and hoop stress are located on zone around the gap tip, as shown in Fig. 10.

Fig. 11(a) shows the total stress components distribution along P1. All the stress components reach the peak value at the zone around the gap tip, and then they decrease to compressive stress away from the gap tip. Fig. 11(b) shows the total stress components distribution along P2. All the stress components reach the peak value at the zone around the weld root, and then they decrease gradually away from the weld root.

5. Discussions

5.1. The difference between total stress and weld stress

At the case without taking welding residual stress into consideration, the stress in tube to tube–sheet joint is low, and the stress in the zone around gap tip is compressive. When the welding residual stress is considered, the stress in the tube to tube–sheet joint is higher, and the stresses in the zone around gap tip are changed into tensile. Based on this result, it can be concluded that the welding residual stress can play a major role in the tube to tube–sheet joint.

5.2. The effect of total stress on SCC

The SCC of austenitic stainless steels may occur when an alloy is simultaneously subject to the tensile stress and a specific corrosive medium. In the failure analysis, the tensile stress is required for the conclusions of SCC. As shown in the paper, the

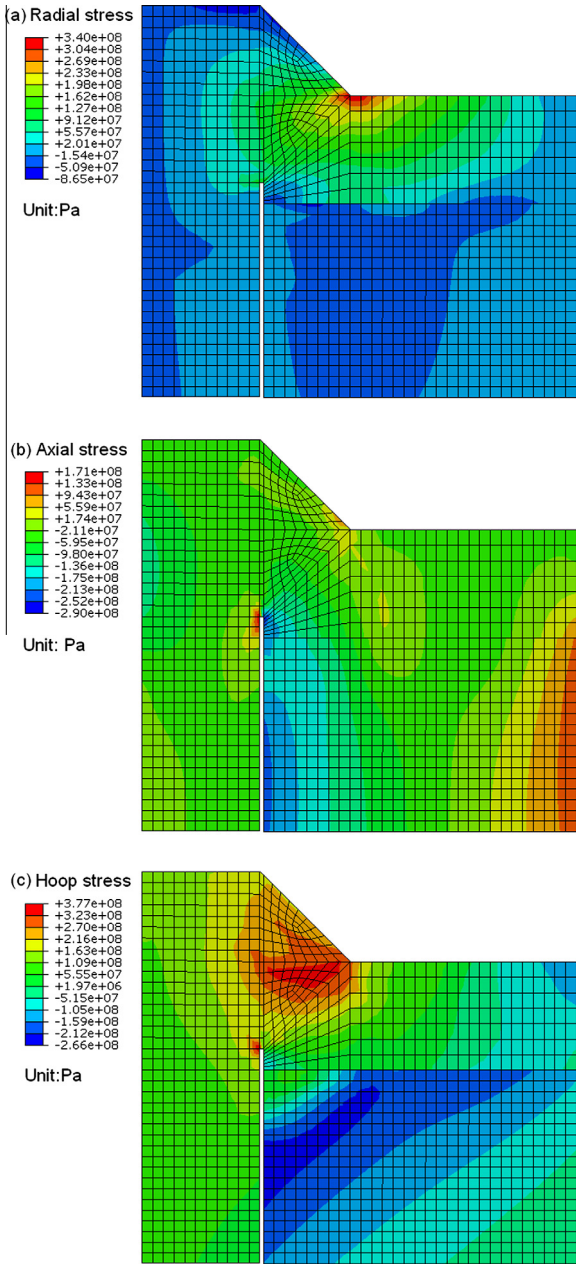

Fig. 10. The total stress contours: radial stress (a), axial stress (b), and hoop stress (c).

thermo-mechanical stress in the generation location of cracks (the vicinity of gap tip) is compressive under the operating temperature and pressure. Once the welding residual stress is applied, the stress state becomes complex, and the total stress in the vicinity of gap tip is tensile. Once this zone faces the sensitive corrosion medium directly, the SCC may occur. Cracks propagated along the axial direction of the tube, which vertical to the radial stress direction. The radial stress in the vicinity of gap tip is tensile. Therefore, controlling the residual stress is very important to assure the structural integrity.

6. Conclusions

Thermo-mechanical stress in tube to tube–sheet joint including the welding effect of a heat exchanger is numerically investigated with an axi-symmetric FE model. The main conclusions can be summarized as follows:

(1) A high tensile stress in the tube to tube–sheet region has been demonstrated by FEM, which is the stress aspect for the SCC phenomenon of austenitic stainless steel in chloride environment.

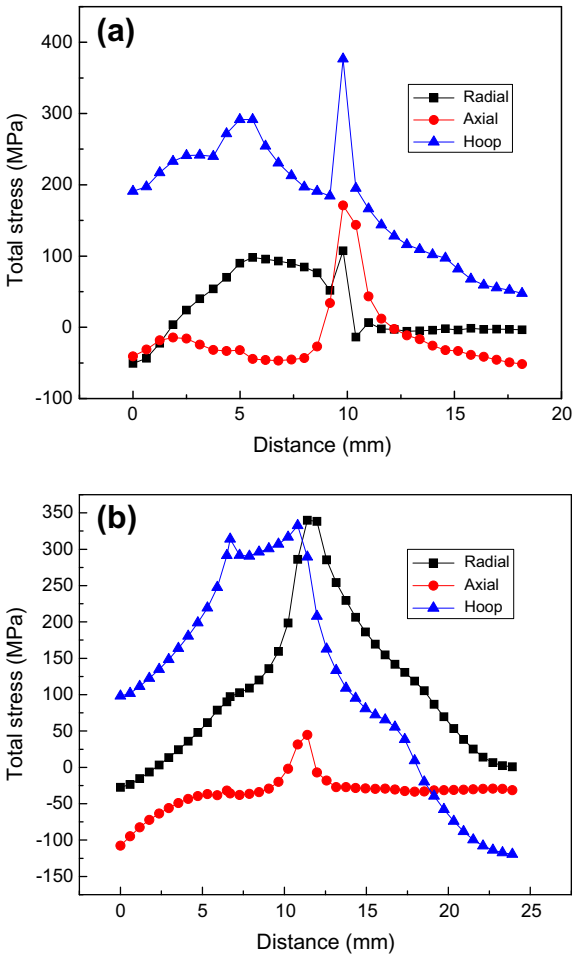

Fig. 11. Total stress distribution along P1 (a) and P2 (b).

(2) The welding, operating temperature, and operating pressure have effect on total stresses. Especially, the welding residual stresses play an important role in the stress state in tube to tube–sheet joint.
(3) Geometric discontinuities of the vicinity of gap cause the welding joint to experience a local stress concentration. High local stresses can cause joints to fail more quickly, so engineers must modify the geometry to minimize stress concentrations.

However, in this paper, a single tube is selected for the analysis of thermo-mechanical stress including welding effect, and welding effect of other tubes around it is ignored. The 3-D FE model of multi-tubes should be considered in future research.

Acknowledgement

This research work was financial supported by the Fundamental Research Funds for the Central Universities (12CX04046A).

References

[1] Merah N, Al-Zayer A. Finite element evaluation of clearance effect on tube-to-tube sheet joint strength. Int J Pres Ves Pip 2003;80(12):879–85.
[2] Xu Shugen, Wang Weiqiang, Liu Huadong. The stress corrosion cracking of austenitic stainless steel heat exchange tubesthree cases study, vol. 5. ASME, Pressure Vessels and Piping Division (Publication) PVP; 2010. p. 33543.
[3] Kim Soon-Tae, Kim Seong-Yoon, Lee In-Sung, Park Yong-Soo, Shin Min-Chul, Kim Young-Sub. Effects of shielding gases on the microstructure and localized corrosion of tube-to-tube sheet welds of super austenitic stainless steel for seawater cooled condenser. Corros Sci 2011;53(8):2611–8.
[4] Azevedo CRF, Beneduce Neto F, Brandi SD, Tschiptschin AP. Cracking of 2.25Cr-1.0Mo steel tube/stationary tube–sheet weldment of a heat-exchanger. Eng Fail Anal 2008;15(6):695–710.
[5] Ghosh Swati, Rana Vishav Preet Singh, Kain Vivekanand, Baveja SK. Role of residual stresses induced by industrial fabrication on stress corrosion cracking susceptibility of austenitic stainless steel. Mater Des 2011;32(7):3823–31.
[6] Nam Jun-Young, Seo Duck-hee, Lee Sang-yun, Hwang Woong-Ki, Lee Bo-Young. The effect of residual stress on the SCC using ANSYS. Proc Eng 2011;10:2609–14.

[7] Tait RB, Press J. An experimental study of the residual stresses, and their alleviation, in tube to tube–sheet welds of industrial boilers. Eng Fail Anal 2001;8(1):15–27.
[8] Meraha N, Al-Zayerb A, Shuaiba A, Arif A. Finite element evaluation of clearance effect on tube-to-tube sheet joint strength. Int J Press Ves Pip 2003;80(12):879–85.
[9] Zain-ul-abdein Muhammad, Nélias Daniel, Jullien Jean-François, Boitout Fréderic, Dischert Luc, Noe Xavier. Finite element analysis of metallurgical phase transformations in AA 6056–T4 and their effects upon the residual stress and distortion states of a laser welded T-joint. Int J Pres Ves Pip 2011;88(1):45–56.
[10] Jiang Wenchun, Liu Zibai, Gong JM, Tu ST. Numerical simulation to study the effect of repair width on residual stresses of a stainless steel clad plate. Int J Pres Ves Pip 2010;88(8):457–63.
[11] Akbari D, Sattari-Far I. Effect of the welding heat input on residual stresses in butt-welds of dissimilar pipe joints. Int J Pres Ves Pip 2009;86(11):769–76.
[12] Xu Shugen, Wang Weiqiang. Numerical investigation on weld residual stresses in tube to tube sheet joint of a heat exchanger. Int J Press Ves Pip 2013;101:37–44.
[13] Becker William T, Shipley Roch J. ASM handbook. Failure analysis and prevention. The Material Information Company; 2002..
[14] Xu Shugen, Wang Weiqiang, Liu Huadong, Zhang Anjun, Tang Jun. Catastrophic explosion of a multilayered urea reactor. Ammonia Plant Saf Relat Facil 2008;49:375–86.
[15] Jiang Wenchun, Xu XP, Gong JM, Tu ST. Influence of repair length on residual stress in the repair weld of a clad plate. Nucl Eng Des 2012;246:211–9.
[16] Liu Hongbing, Tao Jie, Gautreau Yoann, Zhang Pingze, Jiang Xu. Simulation of thermal stresses in SiC–Al_2O_3 composite tritium penetration barrier by finite-element analysis. Mater Des 2009;30(8):2785–90.
[17] Ranjbar-Far M, Absi J, Mariaux G, Dubois F. Simulation of the effect of material properties and interface roughness on the stress distribution in thermal barrier coatings using finite element method. Mater Des 2010;31(2):772–81.